

Abstract. We have obtained a high resolution, high S/N UVES spectrum of the bright QSO HE 2243–6031 to analyze the damped Ly α system (DLA) observed at $z = 2.33$. We measure column densities for H I, N I, Al II, Si II, P II, S II, Ar I, Cr II, Fe II, Ni II, Zn II, C II O I, and Al III; and put upper limits on the abundances of Mn II, S III, Fe III, P III, and N II. **The metallicity of this system is 1/12 solar at a neutral hydrogen column density of $\log N(\text{H I}) = 20.7$. From the observed ratios $[\text{Zn}/\text{Cr}] = -0.01 \pm 0.05$ and $[\text{S}/\text{Si}] = -0.06 \pm 0.03$ we conclude** that dust is **very likely** absent from the ISM of this protogalaxy. We observe an enhancement of the α/Fe -peak ratios of +0.2 dex for various elements, a marked odd-even effect in Mn, and a strong underabundance of N relative to Si and S, $[\text{N}/\text{Si}, \text{S}] = -1$ at $[\text{Si}/\text{H}] = -0.86$. All of these ratios support an environment that is in an early evolutionary stage, where the onset of star formation has begun only shortly before the DLA was observed. We also perform a cloud-by-cloud analysis – without precedent at high redshift – and find a tight correlation of all low-ionization species with respect to Fe II extending over 2.5 orders of magnitude in $N(\text{Fe II})$. We interpret this trend as being due to homogeneous physical conditions (very mild ionization effects, common dust-destruction histories, same chemical composition) and propose that this line of sight encounters absorbing clouds that share a common environment. In addition, photoionization models show that these single clouds are shielded from the external ionizing radiation, so the fraction of ionized gas is small and, except for argon, does not influence the measured metal abundances. The **observed** Al III/low-ion ratios suggest the mildly ionized gas occurs in shells surrounding neutral cores of Al II.

Key words: Cosmology: observations – Quasars: individual: HE 2243–6031 Quasars: general – absorption lines

A&A manuscript no.
(will be inserted by hand later)

Your thesaurus codes are:
missing; you have not inserted them

Metal abundances and ionization conditions in a possibly dust-free damped Ly α system at $z = 2.3^*$

Sebastian Lopez¹, Dieter Reimers², Sandro D’Odorico³, and Jason X.
Prochaska^{4,**}

¹ Departamento de Astronomía, Universidad de Chile, Casilla 36-D, Santiago, Chile.

² Hamburger Sternwarte, Universität Hamburg, Gojenbergsweg 112, 21029 Hamburg, Germany.

³ ESO, Karl-Schwarzschildstr. 1, Garching b. Muenchen, Germany.

⁴ The Observatories of the Carnegie Institute of Washington, 813 Santa Barbara St., Pasadena,
CA 91101, USA.

1. Introduction

Damped Ly α systems (DLAs), defined as those QSO absorption systems with the highest column densities, $N(\text{H I}) > 2 \times 10^{20} \text{ cm}^{-2}$, are widely believed to occur in the ISM of the high redshift progenitors of present-day galaxies (Wolfe 1993). It is fortunate that such large column densities permit very accurate metal abundance measurements because, since DLAs contributed most of the neutral gas mass when the Universe was 10% of its present age (e.g., Storrie-Lombardi et al. 2000), they provide us with a powerful means to trace the chemical evolution of star forming galaxies over a considerable fraction of the Hubble time. Since the absorbing gas in DLAs is expected to be mostly neutral, the bulk of metals should be in neutral or singly ionized form (depending on whether or not the first ionization potential $\text{IP} > 13.6 \text{ eV}$). Thus, the many transitions of these “low ions” that are redshifted to the optical range can be used to compute $[\text{X}^+/\text{H}^0] \approx [\text{X}/\text{H}] \equiv \log(\text{X}/\text{H}) - \log(\text{X}/\text{H})_{\odot}$.

With the advent of 8-10m-class telescopes high resolution spectroscopy of distant QSOs and detailed abundance studies in DLAs have become possible with relatively high accuracy ($\sim 10\%$). The picture that has emerged is that of $Z \sim 1/10 - 1/300 Z_{\odot}$ absorbers with abundance patterns that, **except for the Fe-peak ratios**, resemble that of Milky Way metal-poor halo stars (Lu et al. 1996; Pettini et al. 1997; Prochaska

Send offprint requests to: S. Lopez, slopez@das.uchile.cl

* Based on observations collected at the European Southern Observatory, Chile (Programme ID: 65.O-0411(A))

** Hubble Fellow

& Wolfe 1999; Boisse et al. 1998). These observations seem to support the underlying hypothesis that at least part of the DLAs have undergone a similar chemical evolution history as our own Galaxy.

On the other hand, the observed sub-solar abundances $[X/H]$ observed in the Galactic ISM are interpreted as due to a partial incorporation of the atoms from the gas phase into dust grains (e.g., Savage & Sembach 1996). Since dust is formed through condensation from the gas phase, any measure of the absorbing column density of a refractory element will underestimate the true number of atoms. Moreover, observations of diffuse clouds in the Galactic ISM have shown the clear trend of different elements to condense into grains in different proportions, depending on condensation temperature (Savage & Sembach 1996). Fe, Cr and Ni are among the most depleted elements in the ISM, while O, P, Ar, S, and Zn have generally very small depletion factors. Since DLAs are likely to sample the ISM of galaxies at earlier evolutionary stages, it seems reasonable to raise the question as to whether the measured abundances at high redshift have also been modified by differential dust depletion (e.g., Lu et al. 1996; Pettini et al. 1997). Comparing abundances of refractory and non-refractory elements in high redshift DLAs can lead to estimates of the dust-to-gas ratio in those environments (Pettini et al. 1997; Pettini et al. 1999); assuming particular depletion patterns can in turn be used to correct the measured gas-phase abundances (Vladilo et al. 1998).

However, any assessment of the relative abundances in DLAs is difficult as long as the interplay between dust and nucleosynthesis effects is not well understood, and may not be equal in high redshift DLAs and the local ISM.

The most direct way to disentangle these two contributions to the observed abundance pattern is to find DLAs with as small a level of depletion as possible. Such systems, though, are quite scarce and only few cases are reported in the literature (Molaro et al. 2000; Pettini et al. 2000; Prochaska & Wolfe 1999). **In this paper we present VLT UVES observations of the $z = 3.01$ QSO HE 2243–6031 (discovered by the Hamburg/ESO QSO Survey; Reimers & Wisotzki 1997), and argue that the DLA observed at $z = 2.33$ shows negligible amounts of dust. We have been able to accurately measure abundances for a set of elements of different nucleosynthetic origins and with differing susceptibility to incorporation into dust grains, including the detection of the “rare” elements P and Ar.**

The paper is organized in three parts. First we address the question of the physical conditions in the *single* velocity components and perform a cloud-by-cloud analysis of the relative abundances (§ 4); next we look at the uncertainties introduced by possible ionization effects (§ 5); and the final part (§ 6) is devoted to studying dust-depletion effects and relative abundances. The conclusions are outlined in § 7.

Table 1. UVES Observations of HE 2243–6031

Mode	Wavelength [nm]	Exp. Time [sec]	Observing Date
Dichroic (346+580)	308-388,477-675	14 400	August 4, 5 and 6, 2000
Dichroic (437+860)	376-500,667-1040	10 800	August 8,11 and 12, 2000
Red arm (520)	477-676	3 600	July 10, 1999

2. Observations and data reduction

HE 2243–6031 was observed in service mode with the UVES instrument at the ESO Kueyen telescope in August 2000 under good seeing conditions ($\lesssim 0.8''$). An extra 1-hour exposure had been previously taken during science verification of the instrument. Using two dichroic modes the whole optical range was covered with a total exposure time of 28 800 sec (Table 1).

After bias-subtracting and flat-fielding of the individual CCD frames, the echelle orders were extracted and reduced with self-implemented routines running under MIDAS. The algorithm attempts to reduce the statistical noise to a minimum by fitting the seeing profile with Gaussians. Flux values are assigned with a variance according to the Poisson statistics and the read-out noise, while cosmic-ray hits are assigned with infinite variances. The extraction proceeds in 3 steps: (1) A Gaussian with unconstrained parameters is fitted to the sky profile at each wavelength using the Levenberg-Marquardt method (Press et al. 1986); (2) the variation of width and position with respect to the orders is then fitted along the dispersion direction with low-order polynomials; (3) step (1) is repeated, this time with width and position fixed at the values given by the fit solution, so only the amplitudes can vary.

The extracted orders were wavelength calibrated using as reference Th-Ar spectra taken after each science exposure. All wavelength solutions were accurate to better than typically 1/10 pixel. The wavelength values were converted to vacuum heliocentric values and each order of a given instrumental configuration was binned onto a common linear wavelength scale of $0.043 \text{ \AA pixel}^{-1}$. The reduced orders were then added with a weight according to the inverse of the flux variances. Finally, the flux values were normalized by a continuum that was defined using cubic splines over featureless spectral regions. The spectral resolution is $\text{FWHM} \sim 6.5 \text{ km s}^{-1}$. The typical signal-to-noise ratio varies between $S/N \gtrsim 80$ at 3700–5700 \AA , and $S/N \gtrsim 50$ at 5700–8000 \AA (becoming worse at both ends of the spectrum).

In addition to the UVES data, a low resolution ($\text{FWHM} \approx 4 \text{ \AA}$) spectrum of HE 2243–6031 was obtained on October 12 2001 using the Boller and

Chivens (B&C) Spectrograph on the Baade 6.5m Telescope at Las Campanas Observatory. This spectrum was used to better define the quasar continuum in the spectral region around the damped Ly α line.

3. Line parameters

Column densities N and Doppler parameters b were obtained by fitting Voigt profiles to each velocity component. The fits were performed using the minimum- χ^2 code FITLYMAN (Fontana & Ballester 1995). Since most of the species under study present 2 or more transitions, the results of the fits were in general stable and quite independent of the fitting region chosen.

As an alternative approach to obtain column densities in DLAs, the apparent optical depth method (Savage & Sembach 1991) has been often used to get integrated column densities. The method is straightforward and gives **accurate results for a resolved and non-saturated line** (Lu et al. 1996; Prochaska & Wolfe 1999). In our case, although most of the ions have at least one transition likely not to be saturated, we use instead the fitting approach, because it provides us with better column density estimates of partially blended components, and of those lines having evident departures from the linear part of the curve-of-growth. In addition, unlike previous studies, in which redshift and Doppler parameter of a given velocity component are held fixed for all ions, in our fitting procedure all fit parameters were allowed to vary.¹

The fit results are summarized in Table 2, while the column labeled N_{fit} in Table 3 lists the overall column densities which resulted from summing the individual component column densities. All line parameters come from the Voigt profile fits, with the exception of $N(\text{Zn II})$ and $N(\text{Cr II})$, which were obtained using the apparent optical depth method. Following is a description of the fits to individual species.

3.1. Description of the fits

Fe II. — We begin by fitting Fe II because this is the ion with the most complete set of transitions redward of the Ly α forest. We fitted simultaneously 5 Fe II transitions. They are shown in Fig. 1, plotted in velocity space with respect to $z = 2.330000$, and along with the fitted profiles (smooth line). **The $\lambda 2344$ and $\lambda 2382$ transitions provided a fitting interval only at the position of the weaker components.** We found

¹ Traditionally, line profile fitting of DLA systems has been performed by assuming the same Doppler parameter for all ions at given velocity component, i.e., that bulk motion dominates over thermal motion. This is a reasonable choice as long as DLAs occur in cold gas and the ions under study are massive; however, this does not prevent us *a priori* to chose the free-parameter approach described above.

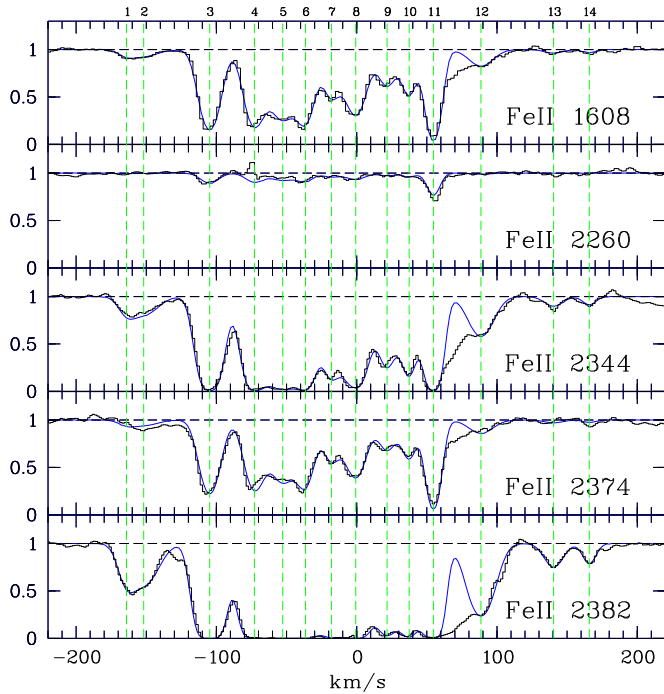


Fig. 1. Velocity plots of observed Fe II transitions (histogram) and fitted profiles. The dashed lines indicate the positions of the fitted velocity components. The zero-velocity point corresponds to $z = 2.330000$.

that 14 velocity components were necessary to model the whole profiles. Their positions are indicated by the vertical dashed lines. We used these line positions to identify – but not to tie – velocity components in the remaining ions and throughout the paper we refer to them as to “C1”, “C2”, etc. We were not able to fit the absorption feature between C11 and C12. There appears not to be enough information on the line profile for FITLYMAN to find the best line centroid. Instead of defining a fixed line position ‘by hand’ we preferred to leave the feature unfitted. An optical depth analysis shows that the contribution to the total Fe II column density should be less than 1%.

Ar I.— We have detected Ar I via the $\lambda 1048$ transition. The $\lambda 1066$ line unfortunately does not provide any useful constraint to the fits. Although the $\lambda 1048$ transition lies in the forest, the spectrum is clean at the expected position of its strongest components. Absorption by Ar I is detected in C3, C4 and C11, which correspond to the three strongest lines in Fe II ($\sim 50\%$ of the total Fe II). **The small line widths suggest these lines are very likely not** due to weak Ly α interlopers. Moreover, the position of the lines match well those of Fe II, with exception maybe of C4, due to blending with a Ly α forest line (which makes the fit an overestimate of $N(\text{Ar I})$ in this component). This is the second ever measurement of argon at high redshift after the $z = 3.39$ detection by

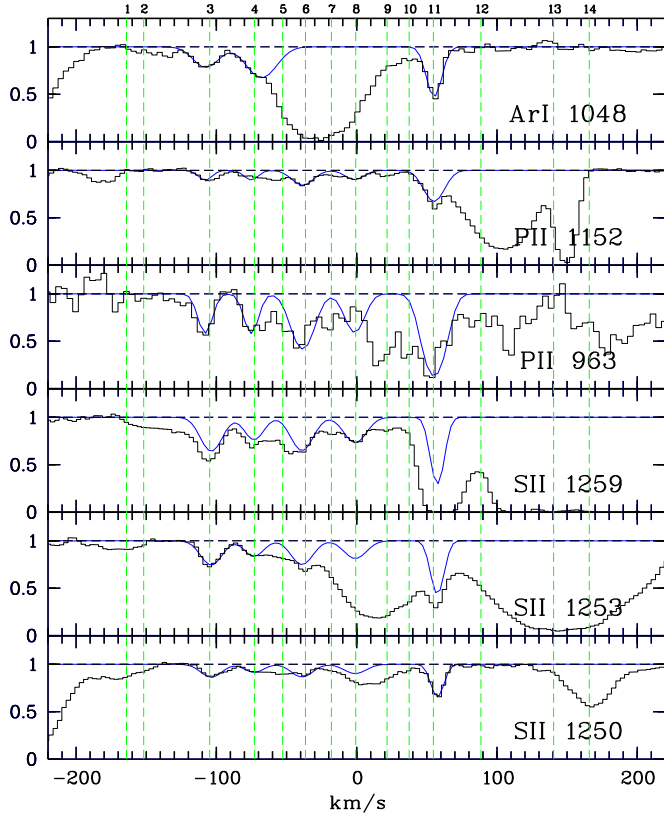


Fig. 2. Same as in Fig. 1 but for the observed Ar I, P II and S II transitions. The dashed lines correspond to the Fe II components.

Molaro et al. (2001), and one of the few outside the Galaxy available (Vidal-Madjar et al. 2000; Levshakov, Kegel & Agafonova 2001).

P II.— We have detected P II via the $\lambda 963$ and $\lambda 1152$ transitions (Fig. 2). We are quite confident of the detection and fit results because they are based on two transitions that happen to fall in a relatively unabsorbed part of the forest. This is only the third detection of extragalactic phosphorus so far (Molaro et al. 2001, Outram et al. 1999). The fits give reasonably good results for C3, C4, C6, and C8. **C11 is blended with a Ly β line at $z = 2.743903$ with $\log N = 14.57$ and $b = 25.1$. These parameters resulted from fitting simultaneously the P II lines, the Ly β , and its corresponding Ly α .**

S II, N I, Si II, Ni II, Al II.— We did not encounter big difficulties by fitting these ions because all of them but Al II show more than one transition, although we were able to fit all 14 components only for Si II. The Al II $\lambda 1670$ line is saturated over most of the components, so column densities of the stronger components must be treated as lower limits. In S II and N I there is obvious blending with forest lines. C1 and C2 in N I were treated as one single component.

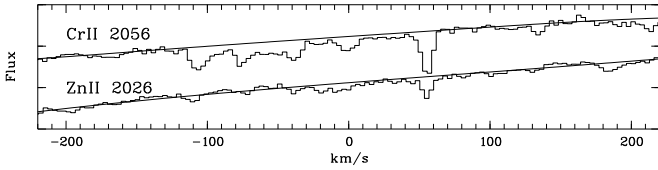


Fig. 3. Portion of the echelle order containing the Cr II $\lambda 2056$ line and portion of one of the orders containing the Zn II $\lambda 2026$. The flux scale was accommodated for displaying purposes, and the zero-velocity point corresponds to $z = 2.330000$.

O I, C II.— For these ions most transitions have saturated components or they lie in the forest, so only a small set of components could be fitted. C3 in C II and C8 in O I are uncertain because of the small fitting interval available. C1 and C2 in O I were treated as one single component.

Mn II.— Mn II is not detected (only the weak $\lambda 2606$ is available, the other transitions falling in the red cross-disperser gap at $\sim 8600 \text{ \AA}$). We derive a 3σ upper limit of $\log N < 11.6$ for a single line. If this value is scaled according to the strongest Fe II component, it gives a total Mn II 3σ limit of $\log N(\text{Mn II}) < 12.43$.

Zn II and Cr II.— To estimate column densities for Zn II and Cr II we used the Zn II $\lambda 2026$ and Cr II $\lambda 2056$ transitions. These are the strongest transitions available and should not be blended with unrelated lines. The $\lambda 2062$ line is partially lost within telluric lines.

Unfortunately, the $\lambda 2026$ and $\lambda 2056$ lines lie in the noisiest part of our spectrum, where spurious features introduced by traces of fringing could not be removed properly. In addition, the Zn II line happens to fall in the overlapping region of two echelle orders, where the continuum definition is inaccurate. This was reflected in the impossibility of profile fitting all components. For this reason we used the apparent optical depth method to constrain the respective column densities. **Integrating between $v = -180$ and $v = +100 \text{ km s}^{-1}$ leads to $\log N(\text{Zn II}) = 12.22 \pm 0.03$ and $\log N(\text{Cr II}) = 13.24 \pm 0.02$. We have excluded the velocity region $[+100, +180]$, due to spurious features that introduce extra noise (excluding C13 and C14 introduces an uncertainty no larger than $\sim 0.5\%$, though). We stress, however, that due to the weakness of the lines these values are subject to continuum uncertainties (which are not considered in the formal errors).**

Doubly ionized species.— Fig. 7 displays the expected position in velocity space of all doubly ionized species covered by our spectrum. **N II is also included in the figure.** It is of great importance to estimate or put useful limits on column densities for these ions, as they will constrain the ionization level of the system.

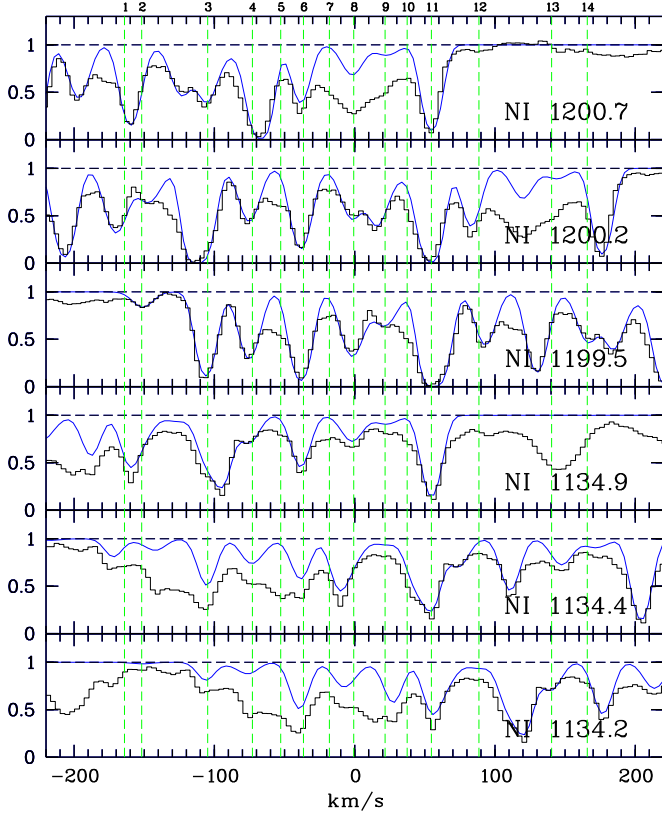


Fig. 4. Same as in Fig. 2 but for the observed Ni I transitions.

For Al III we have at our disposal two transitions with apparently unsaturated lines, so the fit results can be considered reliable. Note that C13 and C14 are not detected.

For the rest of the ions we have attempted to put upper limits on column densities using different approaches. For S III we use the transition at $\lambda = 1012 \text{ \AA}$. Although the line lies in the forest, there is a relatively good match of the absorption profile with that of Fe II, in line position as well as in line strengths. This suggests the S III is present in the DLA gas and tracks the low-ion profiles. However, since the lines stand out only poorly we did not attempt a fit; instead, we used the total apparent column density, which gives $N(\text{S III}) = 14.05 \pm 0.01$ for $v = [-130, +80]$.

To constrain Fe III we use the $\lambda 1122$ transition. This line is also in the forest and appears so severely contaminated that no resemblance with Al III or low-ion profiles is recognized. An upper limit was estimated by assuming a Fe III line lies at C3 and has $b = b_{\text{Fe II}} = 8.0 \text{ km s}^{-1}$. The maximum column density allowed by the data then becomes $\log N = 13.4$, which, weighted with C3 from the Al III fits yields a total column density of $N(\text{Fe III}) < 14.18$. Note, however, that the Fe III profile does not exclude $N(\text{Fe III}) = 0$.

For P III we performed the same exercise using the expected position of the $\lambda 998$ transition, which also shows no black absorption. At C3 we get $\log N(\text{P III}) < 13.2$ for $b = 8.4 \text{ km s}^{-1}$, or $\log N(\text{P III}) < 13.98 \text{ cm}^{-2}$ for the whole profile. Again, since the line is

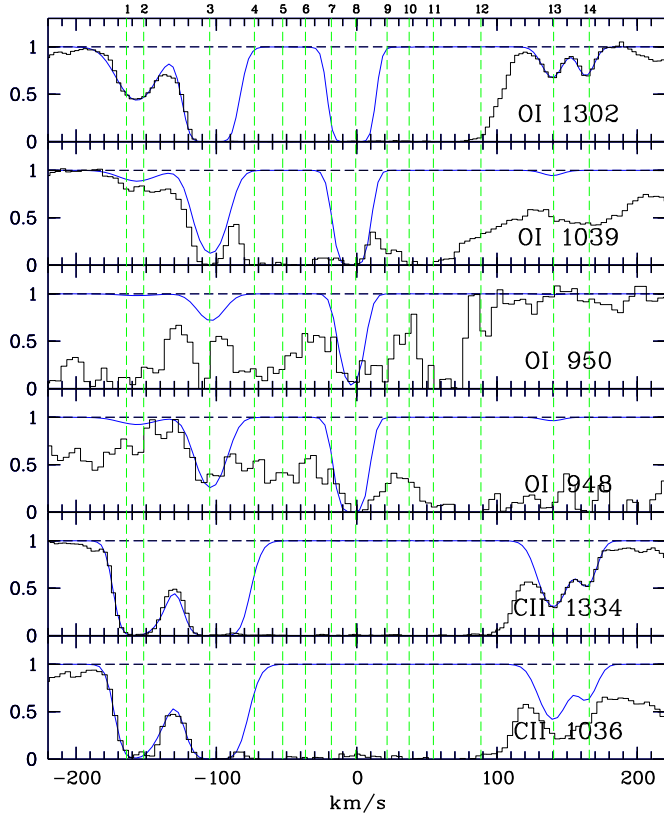


Fig. 5. Same as in Fig. 2 but for the observed O I and C II transitions.

in the forest and we do not recognize an Al III-like absorption pattern, we cannot exclude $N(\text{P III}) = 0$.

Finally, the $\lambda 1083$ profile, despite forest contamination, also resembles the low-ion pattern. This is interesting given that nitrogen is expected to be mainly neutral due to its high IP of 14.5 eV. Assuming that the absorption feature at C11 is a N II $\lambda 1083$ line and weighting with C11 from the Al III fits we estimate that $N(\text{N II}) < 14.55$.

3.2. Neutral hydrogen column density

Despite its high S/N and coverage of higher order Lyman series lines, obtaining $N(\text{H I})$ from the UVES spectrum alone posed some difficulties owing to the non-Voigt shape of the damped Ly α line. To estimate $N(\text{H I})$ we used instead the B&C spectrum, where the fit to Ly α was much better constrained than in the high resolution spectrum. This shows the difficulties of defining a continuum around an absorption feature that extends over several echelle orders.

We fitted the damped Ly α line with 14 individual components whose positions were fixed at the Fe II velocity components. The H I column density was

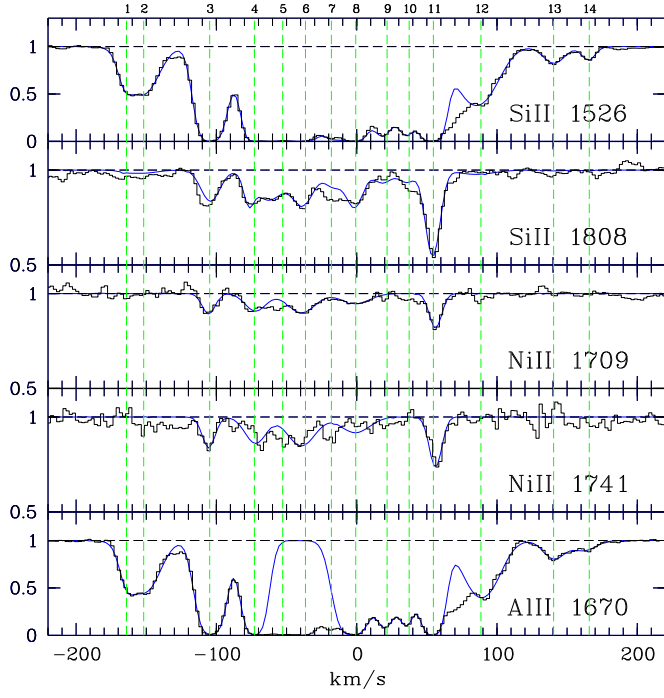


Fig. 6. Same as in Fig. 2 but for the observed Si II, Ni II and Al II transitions.

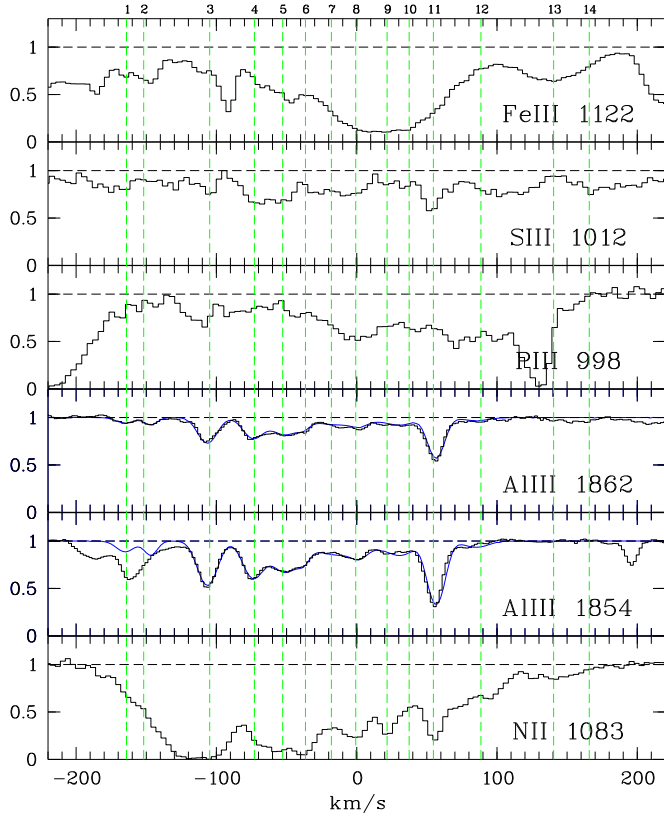


Fig. 7. Same as in Fig. 2 but for doubly ionized species and N II. The absorption feature at $v = -90 \text{ km s}^{-1}$ in the top plot is unrelated from Fe III 1122.

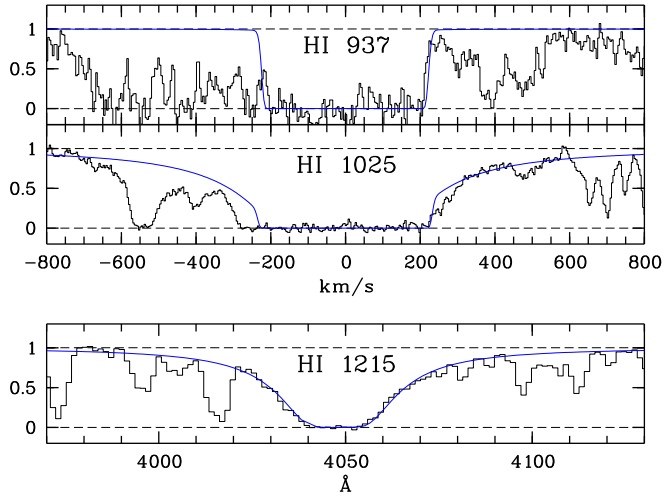


Fig. 8. UVES (top panels) and B&C spectrum of HE 2243–6031 at the position of the H I lines used to constrain $N(\text{H I})$. The smoothed line is the superposition of 14 H I velocity components centered at the positions of the Fe II lines. The individual H I column densities are proportional to the Fe II column densities, and the total H I column density $\log N(\text{H I}) = 20.67 \text{ cm}^{-2}$. The Doppler parameter b is assumed to be the same for all components and has the value of $b = 16 \text{ km s}^{-1}$, as constrained by Ly β and Ly ϵ .

varied as to keep the $N(\text{Fe II})/N(\text{H I})$ ratio constant for all components, and the b -parameter was assumed the same for all components. The best fit we obtained implies an overall column density of $\log N(\text{H I}) = 20.67 \pm 0.02 \text{ cm}^{-2}$. Since the same value is obtained if a single fit component is assumed, we conclude that the assumption of constant Fe II/H I is unimportant in so far as the $N(\text{H I})$ value is concerned. The fitted profiles are shown in Fig. 8.

We note that the fit solution still leaves underabsorbed “voids” in the blue wings of the Ly β line. These are produced by low column-density Ly α systems that do not show the low-ionization species studied in this paper.

Of course the underlying assumption in our fitting procedure that Fe II/H I remains constant over all velocity components, although expected if the gas is well mixed, must not hold if Fe II is for instance inhomogeneously dust depleted. Next section deals with such possible variations.

4. Inferences from cloud-to-cloud variations

In this section we investigate cloud-to-cloud variations of the relative abundances. There are 3 possible sources of abundance variations among clouds: (1) differential depletion due to differing composition and destruction histories of dust grains; (2) different ionization

Table 2. Line parameters

Ion	Comp.	z	$\log N(\sigma_{\log N})$ cm ⁻²	$b(\sigma_b)$ km s ⁻¹	Ion	Comp.	z	$\log N(\sigma_{\log N})$ cm ⁻²	$b(\sigma_b)$ km s ⁻¹
C II	1	2.328224	14.35 0.02 ^a	9.4 0.2	S II	3	2.328849	14.17 0.01	9.5 0.5
	2	2.328370	14.04 0.01 ^a	12.9 0.2		4	2.329187	13.91 0.07	8.4 1.9
	3	2.328879	14.81 0.10 ^a	15.5 1.8		6	2.329567	14.17 0.03	9.7 0.9
	13	2.331557	13.76 0.01	11.9 0.4		8	2.329989	14.04 0.04	10.1 1.4
	14	2.331823	13.34 0.02	8.0 0.4		11	2.330639	14.43 0.01	4.9 0.3
N I	1+2	2.328322	12.87 0.04	9.2 1.2	Ar I	3	2.328805	12.89 0.04	11.5 1.4
	3	2.328823	13.90 0.01	7.3 0.1		4	2.329247	13.17 0.13	13.6 4.2
	4	2.329165	13.68 0.01	8.3 0.2		11	2.330613	13.17 0.02	5.7 0.5
	6	2.329573	14.01 0.00	7.5 0.1	Fe II	1	2.328177	12.51 0.016	6.8 0.0
	8	2.329980	13.68 0.01	9.1 0.3		2	2.328314	12.86 0.008	12.8 0.0
	9	2.330252	13.21 0.03	10.3 1.2		3	2.328836	14.09 0.003	8.0 0.0
	11	2.330590	14.40 0.01	7.0 0.1		4	2.329190	14.03 0.003	7.9 0.0
O I	1+2	2.328260	14.18 0.01	16.9 0.4	5	2.329414	14.04 0.003	10.6 0.0	
	3	2.328844	15.28 0.04	12.0 0.2	6	2.329595	13.92 0.004	6.9 0.0	
	8	2.329960	16.15 0.30 ^a	7.4 1.2	7	2.329800	13.60 0.005	6.9 0.0	
	13	2.331549	13.60 0.01	8.9 0.4	8	2.329993	13.91 0.003	8.7 0.0	
	14	2.331820	13.45 0.01	6.0 0.3	9	2.330241	13.45 0.005	7.1 0.0	
	Al II	1	2.328179	11.76 0.03	5.1 0.3	10	2.330415	13.52 0.005	5.7 0.0
2		2.328313	12.40 0.01	13.5 0.2	11	2.330608	14.31 0.006	4.8 0.0	
3		2.328846	13.03 0.01 ^a	8.8 0.1	12	2.330984	13.20 0.005	11.0 0.0	
4		2.329190	13.07 0.06 ^a	7.2 0.3	13	2.331559	12.39 0.018	8.2 0.5	
8		2.329967	13.14 0.02 ^a	10.5 0.5	14	2.331842	12.17 0.025	5.2 0.6	
9		2.330226	12.64 0.02	6.8 0.4	Ni II	3	2.328828	13.00 0.03	5.1 0.6
10		2.330395	12.56 0.02	5.7 0.4		4	2.329200	13.15 0.11	9.5 2.6
11		2.330601	13.21 0.05 ^a	6.3 0.3		6	2.329562	13.30 0.06	12.8 2.2
12		2.330989	12.50 0.01	15.1 0.3	8	2.329989	13.04 0.10	13.5 4.0	
13		2.331562	11.69 0.04	9.4 0.8	11	2.330624	13.24 0.02	4.7 0.4	
14	2.331798	11.47 0.06	11.2 1.5	Al III	1	2.328165	11.82 0.09	7.8 2.7	
Si II	1	2.328164	12.83 0.05		4.8 0.5	2	2.328366	11.82 0.08	5.1 1.6
	2	2.328302	13.55 0.01		13.8 0.3	3	2.328815	12.57 0.01	8.4 0.2
	3	2.328842	14.38 0.01		8.4 0.1	4	2.329176	12.47 0.01	8.9 0.3
	4	2.329145	14.04 0.06		2.9 0.8	5	2.329428	12.50 0.02	12.5 0.6
	5	2.329301	14.56 0.02		13.9 0.5	6	2.329579	11.67 0.11	4.2 1.3
	6	2.329574	14.48 0.02		9.6 0.4	7	2.329858	12.40 0.07	24.3 4.3
	7	2.329815	14.04 0.03		7.5 0.6	8	2.330019	11.68 0.09	6.4 1.5

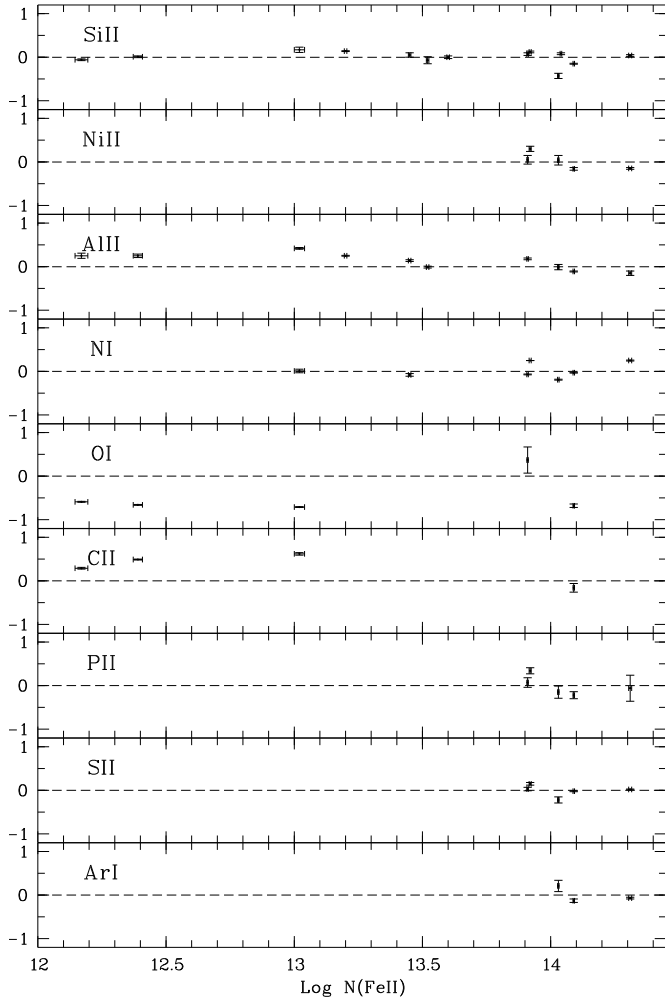


Fig. 9. $\log N_i(X)/N_i(\text{Fe II}) - \log N_{\text{corr}}(X)/N_{\text{corr}}(\text{Fe II})$ vs. $\log N_i(\text{Fe II})$ of all observed low-ion velocity components. N_{corr} denotes the total, corrected column densities listed in Table 3.

conditions due to density variations and/or local changes in the ionization field (§ 5); and (3) simply differing chemical compositions.

4.1. No abundance gradients

Fig. 9 plots $\log N_i(X)/N_i(\text{Fe II})$ versus $\log N_i(\text{Fe II})$ for all velocity components for which column densities and associated errors are available. In each panel the values have been normalized by $N_{\text{corr}}(X)/N_{\text{corr}}(\text{Fe II})$, where N_{corr} is the total column density listed for each element in Table 3. Since we were not able to obtain individual component values of $N(\text{Zn II})$ we use instead $N(\text{Fe II})$ as reference, bearing in mind that iron is possibly subject to differential dust depletion. C1 and C2 have been integrated and treated as a single component due to possible blending that could have affected the fits; the new value corresponds to the point at $\log N(\text{Fe II}) = 13.02$.

From Fig. 9 we see that the $N(X)/N(\text{Fe II})$ ratio remains, within measurement errors, fairly constant over almost two and half orders of magnitude in $N(\text{Fe II})$. This is specially evident in Si II, for which we have the most robust column density estimates and coverage of all Fe II components. The same trend holds even for those ions for which we were able to obtain N only for the strongest components (Ni II, N I, P II, S II, Ar I). The major discrepancies with respect to the assumed abundances are found in O I and C II, but these are easily explained by the saturated C3 in both transitions used for C II, and by the overfitted C8 in O I. Al II also shows discrepant values between weak and stronger components; this is most likely due to saturation effects affecting the fits to high column densities components (which underestimate the true $N(\text{Al II})$).

From the data on Si II we deduce that the single column densities diverge from the assumed value $\log N(\text{Si II}) = \log N(\text{Fe II}) + 0.44$ on average by only 0.15 dex. The constancy of $N(\text{Si II})$ over such wide range of Fe II column densities has important implications for this DLA. First, silicon is an α -element. If the delayed injection of processed material from SN Type I and II had undergone differing histories from cloud to cloud, one would expect such variations to be reflected in the individual Si II/Fe II ratios; indeed, we would expect to observe as large a scatter in Si II/Fe II as the dispersion observed among different DLAs of the same metallicity (e.g., Lu et al. 1996). Secondly, silicon is a refractory element. Locally, the depletion of Si and Fe differ by much larger factors than what is observed here, over all ISM environments from the cool disk to the warm halo (Savage & Sembach 1996). In addition, since the gas-phase abundances of refractory elements decrease with $\log \text{H I}$ (e.g., Wakker & Mathis 2000) – and thus with $\log N(\text{Fe II})$ in this DLA – we would expect departures from the assumed abundances at higher values of $\log N(\text{Fe II})$. Altogether, the small variations we observe in Fig. 9 mean both the chemical evolution in single clouds has been the same, and dust is either absent or has different properties from the ISM. Such small variations have been pointed out just for one other DLA (Prochaska & Wolfe 1996) toward Q0201+365 at $z = 2.5$. Those authors also suggested the absence of dust could explain their observations. The novelty of our approach is that we present the first cloud-by-cloud analysis where that trend is observed (instead of integrating the column densities over particular velocity windows). From an instrumental point of view, the homogeneous behavior of these abundances imply the $N(\text{Fe II})$ -weighted corrections that we will apply to some of the low-ion column densities are physically acceptable.

The behavior we see in this DLA has not been observed in the local ISM, which shows a range of values of roughly 1 dex (Spitzer & Fitzpatrick 1995; Welty et al. 1999), nor in the LMC (Welty et al. 1999). It is well known that such lines of sight probe regions in different environments; therefore, it seems conceivable that this DLA encounters an homogeneous population of clouds.

Under the assumption that Fe II tracks H I this line of sight probes the interval $\log N(\text{H I}) \approx 18 - 20 \text{ cm}^{-2}$, which, if in our Galaxy, would mean probing a mixture of halo and disk clouds (Wakker & Mathis 2000; and references therein). Wakker & Mathis (2000) find a remarkable anticorrelation of the metal abundance with H I in the local ISM, which they interpret as the environmental dependence expected if both disk (with low gas-phase abundances) and halo (with high gas-phase abundances) are plotted together as a function of H I. Our observations do not fit into this scenario, as – again assuming $N(\text{H I}) \propto N(\text{Fe II})$ – they show no dependence of abundances with respect to H I column density (Fig. 10). Two possible explanations may be responsible for this discrepancy: (1) Fe II simply does not track H I but is an increasing function of H I, in which case, a higher density cloud would have a higher metallicity; or (2) this particular line of sight probes just one type of environment. The above discussion seems to support the second alternative.

5. Ionization

If high redshift DLAs occur in dense protogalactic clumps, then one can expect a soft ionizing radiation field which is not able to penetrate gas with $N(\text{H I}) > 10^{20} \text{ cm}^{-2}$. As a result, all elements but those having their first ionization potential $> 13.6 \text{ eV}$: N I, O I, Ar I, should be primarily in singly ionized form, with little gas in ionized form (e.g., Viegas 1995). More recently, several authors have investigated the systematic effects of ionized gas on the determination of metal abundances from the low-ionization species (e.g., Howk & Sembach 1999; Vladilo et al. 2001).

In the present DLA the moderately low overall $N(\text{H I})$, and the detection of some doubly ionized ions such as Al III having similar velocity profiles as their singly ionized counterparts, both suggest ionization may play a role in bringing part of the low ions to a higher, in principle undetectable ionization level. In this section we argue against ionization affecting considerably our measurements of the metal abundances even for the *single* clouds.

5.1. Self-shielding

Our observations suggest that H I is distributed over all of the single components. Under the assumption $\log N(\text{H I}) = \log N(\text{Fe II}) + 5.75$ for each of the velocity components, the median value of an H I cloud is derived to be $\log N(\text{H I}) = 19.26$, i.e., at least half of the clouds would be considerably ionized, were they part of a classical Lyman-limit system (e.g., Lopez et al. 1999). Given the complexity of the present system, however, it is also conceivable that self-shielding does keep the single clouds in a more neutral environment. Evidence for this comes from the constancy of the low-ion/Fe II ratio down to the lowest

measurable Fe II column densities. Fig. 10 shows the ratio $\log(N(\text{Si II})/N(\text{Fe II}))$ as a function of $\log N(\text{Fe II})$. The Si II/Fe II ratio *of integrated column densities* in DLAs should be only mildly influenced by ionization effects (Vladilo et al. 2001; Howk & Sembach 1999). We interpret the datapoints in Fig. 10 as an extension of that property down to much lower densities, thus suggesting self-shielding in the present system.

Next, to address the question of how ionization may influence the single-cloud abundance ratios, we compare the fit results for the single components of Fe II and Al III, which are good proxies for the low and medium-ionization gas, respectively. As for Fe II, Al III column densities also fulfill the requirement of coming from unsaturated and resolved lines. Ideally, we would have liked to have used Al II instead of Fe II to disentangle the effect of possible variations in the relative abundances (despite the results shown in § 4), but the former ion has only one transition ($\lambda 1670$), and some of the components are saturated. Triply ionized species such as C IV or Si IV were not used as their profiles indicate they occur in distinct volumes. Fig. 11 shows the ratio $\log(N(\text{Fe II})/N(\text{Al III}))$ as a function of $\log N(\text{Fe II})$ for all 12 velocity components for which column densities and associated errors are available. The two lower limits correspond to the non-detection of Al III at the positions of C13 and C14, and the dashed line mark the Fe II/Al III calculated from the overall column densities. We use the same y-scale as in Fig. 10 to permit a comparison of the scatters. Contrary to the constant behavior of the $N(\text{Si II})/N(\text{Fe II})$ ratio, there is a larger scatter in $N(\text{Fe II})/N(\text{Al III})$ of about 1 dex over the same interval in $N(\text{Fe II})$. Given the constancy in the low-ion abundances, such scatter could be attributed to cloud-to-cloud variations in ionization.

Our $\log N(\text{Al III})/N(\text{Al II}) \lesssim -0.6$ is typical of DLAs with similar $N(\text{H I})$, according to the compilation by Vladilo et al. (2001). These authors find an empirical anti-correlation between $N(\text{H I})$ and the Al III/Al II ratio, suggesting that H I indirectly traces the level of ionization in the gas. A similar trend is not seen in our Fe II/Al III plot. We find that the two points representing the most ionized clouds (**i.e., lowest Fe II/Al III ratio; corresponding to C1+C2 and C7**) contribute only 17 % (6%) of the total Al III (Fe II) column density. Ignoring those two datapoints we find that Fe II/Al III remains **in this DLA** quite independent of Fe II (and thus of H I in the single clouds). A linear regression analysis gives a slope of only $m = 0.16 \pm 0.32$, which, should Fe II indeed track H I over these interval, is small when compared with the $m = 0.81 \pm 0.015$ found by Vladilo et al. (2001) for larger H I column densities. The conclusion again is that this system, although made of several individual absorbing clouds, can be treated as one single cloud exposed to the ionizing radiation. This is basically the same conclusion reached by Prochaska & Wolfe (1996) for the $z = 2.5$ DLA. Let us also note that a constancy of the ionization

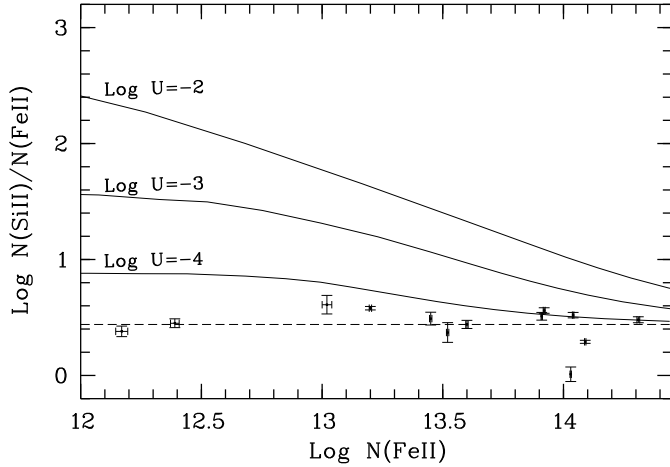


Fig. 10. Observed ratio $\log N(\text{Si II})/N(\text{Fe II})$ vs. $\log N(\text{Fe II})$ along with measurement errors. The dashed line mark the assumed ratio from the overall Si II and Fe II column densities. The solid curves are CLOUDY simulations for an extragalactic ionizing field and for $[\text{Fe}/\text{H}] = -1.0$ and $[\text{Si}/\text{Fe}] = +0.4$.

conditions is similarly observed in the local ISM through the small variability of ionized helium (Wolff, Koester & Lallement 1999).

5.2. Spatial distribution of Al III

Fig. 11 also provides hints on the spatial distribution of Al III. In view of our finding that the low-ionization species in this DLA track each other independently of gas density, if Al III is co-spatial with the low ions then we expect that they anticorrelate, because a decrease in H I (low-ion) column density implies an increase in ionization. Since little dependence of Al III with Fe II is observed, we conclude that a scenario of partially ionized clouds (i.e., with Al III occurring in partially ionized interfaces bordering the neutral gas) is more plausible than co-spatiality.

In such a scenario one would expect from the line widths to observe no correlation between Al III and Al II b -values. We obtain a dispersion of $\sigma \equiv \sqrt{\sum (\Delta b)^2 / 11} = 1.94$ km s^{-1} for Al II–Al III, while $\sigma = 1.1$ km s^{-1} for Al II–Fe II, and 0.7 km s^{-1} for Fe II–Si II (including C13 and C14). If real, these differing dispersions are indicative of absorption occurring in different regions.²

² We stress, however, the potentially large systematic errors that may be present in our measurements of b , especially due to saturation of some Al II components.

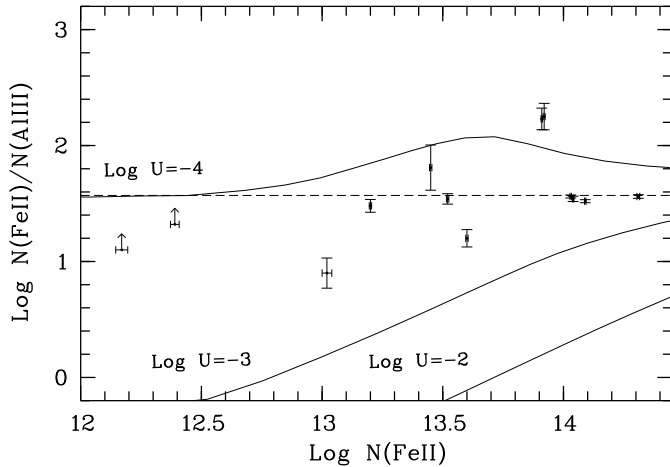


Fig. 11. Same as in Fig. 10 but for the ratio $\log N(\text{Fe II})/N(\text{Al III})$.

5.3. Photoionization models

We performed photoionization models for this DLA and compared the simulations with the observed Si II, Fe II, and Al III in order to establish the level of ionization of each *single* cloud. The simulation outputs were also used to quantify possible (if any) ionization corrections to the observed relative abundances.

We used the code CLOUDY (Ferland 1993) to model the ionization state for a range of H I column densities and ionization parameters (U , the ratio of ionizing photons to the total hydrogen number density). CLOUDY gives column densities for a given set of the input parameters: gas metallicity Z , gas number density n_{H} , and ionizing spectrum J_{ν} . Of these, shape and intensity of the ionizing spectrum introduce the major uncertainties. We adopted the universal background ionizing field due to QSOs and galaxies calculated in Haardt & Madau (1996; an electronic, updated version was kindly provided by the authors). This is the appropriate choice for our treatment of the individual clouds as isolated objects embedded in an intergalactic field. Stars as sources of photoionization are not likely to influence significantly these models: again referring to the work by Prochaska & Wolfe (1996) the exponential fall off of a blackbody ionizing flux has a similar shape as the He II Lyman-break in the Haardt & Madau spectrum for the energy range of interest. The intensity of the field at the Lyman-limit was taken to be $J_{912} = 4.4 \times 10^{-22}$ ergs $\text{s}^{-1} \text{cm}^{-2} \text{Hz}^{-1} \text{sr}^{-1}$ at $z = 2.3$ (consistent with results obtained using the proximity effect; e.g., Giallongo 1996). The geometry was plane parallel and illuminated from one side. The metallicity was fixed at $[\text{Fe}/\text{H}] = -1.0$, and the relative abundances of interest $[\text{Si}/\text{Fe}]$ and $[\text{Fe}/\text{Al}]$ were fixed at the values listed in Table 3. For fixed values of U we ran a grid of models by varying $N(\text{H I})$ in steps of 0.2 dex. Each integration was stopped when the required H I value was reached. (i.e., the cloud size scales with H I in order

to keep U constant). The smoothed curves in figures 10 and 11 show the results of the simulations for $\log U = -2, -3, \text{ and } -4$.

Fig. 10 shows that in our model even at the very lowest ionization parameters a mild but significant increase of the Si II/Fe II ratio with decreasing Fe II is expected. Compared to the model, the datapoints confirm that the behavior of the observed Si II/Fe II ratio is not consistent with isolated clouds, and that some degree of self-shielding must exist in order to keep this ratio constant over the observed range of Fe II column densities. We warn that the H I value at which the iterations are stopped to obtain a given (Fe II, Si II/Fe II)-point is systematically lower than our assumed $\log N(\text{H I}) = \log N(\text{Fe II}) + 5.75$. In other words, Fe II is not tied to H I in this model for $N(\text{Fe II}) < \sim 13.5 \text{ cm}^{-2}$. The simulated Fe II values are indeed obtained for systematically higher H I column densities than the assumed from the observed Fe II values. However, this fact and the use in the simulations of slabs illuminated just from one side both support the notion that *i*) the individual clouds are embedded in a more neutral environment than if they were isolated, and *ii*) the ionization is homogeneous over the DLA components. In consequence, treating the system as one single cloud with $N(\text{H I}) = 20.67$ should not introduce major systematic errors.

Concerning Al III, note that all but 2 points in Fig. 11 lie within the contours $\log U = -4$ and -3 , while all Si II measurements are explained with $\log U < -4$. If different ionization conditions explain the data, then Al III and Si II (and so Al II) may occur in spatially distinct regions.

Finally, Fig. 12 considers the same photoionization models but with $N(\text{H I}) = 20.67$. The vertical axis now shows the ratio $N(\text{X}^i)/N(\text{X}^{i+1})$ for the variety of observed ions as a function of U . The thick sections of the curves indicate those regions allowed by the 3σ upper limits on the doubly ionized species Al III, Fe III and S III. The softer limit is set by Al II/Al III, but recall that Al II is probably underestimated due to mild saturation. **Assuming $\log U \approx -3.8$, this plot shows the approximation $[\text{X}/\text{H}] \approx [\text{X}^+/\text{H}^0]$ should be accurate for the present DLA to within $\sim 5\%$, with the exception of Ar, which is still primarily ionized in this regime.**

6. Metal abundances

6.1. Corrections to column densities

For all ions but Fe II and Si II, we were not able to determine column densities of each of the 14 velocity components. For weak transitions in noisy parts of the spectrum only the stronger components could be fitted, while for strong transitions only the weakest components were accessible due to blending of the saturated components. For those incomplete fits we applied a correction by scaling the summed column densities according

Table 3. Low ions: Total column densities and abundances

Ion	f^a	$\log N_{\text{fit}}^b$	$\log N_{\text{corr}}^c$	$[\text{X}/\text{H}]^d$
H I 1215	0.41640	20.67(0.02)		
C II 1036	0.12310	>15.02(0.06)	>15.80	>-1.43 0.08
C II 1334	0.12780			
N I 1199	0.13280	14.76(0.003)	14.88	-1.84 0.02
N I 1200.2	0.08849			
N I 1200.7	0.04423			
N I 1134.1	0.01342			
N I 1134.4	0.02683			
N I 1134.9	0.04023			
O I 1039	0.00904	16.21(0.19)	16.79	-0.81 0.21
O I 1302	0.04887			
O I 950	0.00157			
O I 948	0.00645			
Al II 1670	1.81000	>13.83(0.02)	>13.97	>-1.18 0.04
Si II 1808	0.00256	15.36(0.02)	15.36	-0.86 0.04
Si II 1526	0.12700			
P II 1152	0.23600	13.28(0.08)	13.42	-0.82 0.10
P II 963	1.46000			
S II 1250	0.00545	14.88(0.01)	15.02	-0.92 0.03
S II 1253	0.01088			
S II 1259	0.01624			
Ar I 1048	0.24400	13.57(0.05)	13.85	-1.38 0.07
Cr II 2056	0.10500	13.24(0.02) ^e		-1.11 0.09
Mn II 2606	0.19270	<11.6	< 12.43	<-1.77
Fe II 1608	0.05850	14.92(0.003)	14.92	-1.26 0.02
Fe II 2260	0.00244			
Fe II 2344	0.11420			
Fe II 2374	0.03131			
Fe II 2382	0.30000			
Ni II 1709	0.03240	13.86(0.03)	14.00	-0.92 0.05
Ni II 1741	0.04270			
Zn II 2026	0.48900	12.22(0.03) ^e		-1.10 0.05

^a Oscillator strengths taken from Morton (1991) for H I, C II, N I, P II, S II, Ar I, and Mn II; from Verner et al. (1994) (updated values) for O I, Al II, Al III, and S III; from Schectman et al. (1998) for Si II λ 1526; from Bergeson & Lawler (1993b) for Si II λ 1808; from Bergeson & Lawler (1993a) for Cr II and Zn II; from Fedchak et al. (2000) for Ni II; from Howk et al. (2000) for Fe II λ 1608, 2260, 2344, and 2374; and from Cardelli & Savage (1995) for Fe II λ 2382.

^b Overall column densities from Voigt-profile fits. For C II, O I, and Al II at least one component was saturated in all transitions available.

^c Column densities corrected for non-fitted components using weights given by the individual

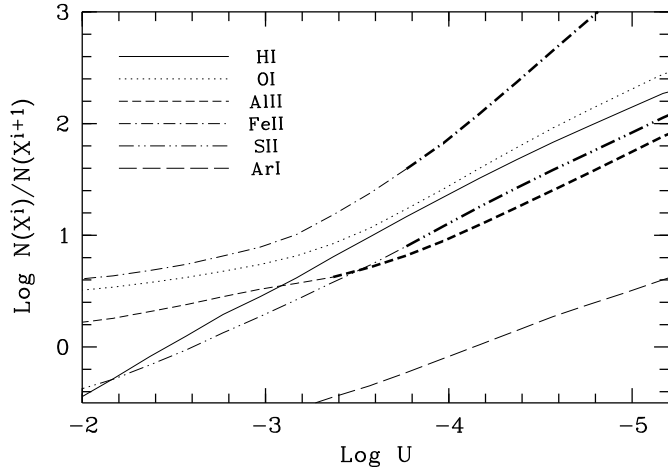


Fig. 12. Expected column density ratios as a function of ionizing parameter U for $\log N(\text{HI}) = 20.67$ and a Haardt & Madau (1996) ionizing field.

Table 4. High ions

Ion	f^a	$\log N_{\text{fit}}$	$\log N_{\text{corr}}^c$
Al III 1862	0.28600	13.35(0.01) ^b	13.35
Al III 1854	0.57500		
S III 1012	0.04250	<14.05 ^d	<14.05
Fe III 1122	0.07884	<13.40 ^e	<14.20
P III 998	0.11200	<13.20 ^f	<14.00
N II 1083	0.10310	<13.95 ^g	<14.55

^a Oscillator strengths taken from Morton (1991) for Fe III and N II; from Verner et al. (1994) for S III, P III and Al III.

^b Overall column density from Voigt-profile fits.

^c Column densities corrected for non-fitted components using weights given by the individual $N(\text{Al III})$ -values

^d Column density limit derived from the apparent-optical-depth method

^e Column density limit derived from Voigt profile of C3 assuming $b_{\text{Fe II}} = b_{\text{Fe III}}$

^f Column density limit derived from Voigt profile of C3 assuming $b_{\text{P II}} = b_{\text{P III}}$

^g Column density limit derived from Voigt profile of C11 assuming $b_{\text{N I}} = b_{\text{N II}}$

to the results for Fe II. We have shown in the previous section that this approach is acceptable in this DLA. The corrected values are listed in the column labeled N_{corr} of Table 3. Since for weak transitions the strongest components dominate the total column densities, the corrections are small and should not introduce large uncertainties; on the contrary, intrinsically strong transitions with only weak components fitted (O I and C II), should suffer from systematic errors, and must thus be taken cautiously.

6.2. Metallicity of the DLA gas

Taking the non-refractory element Zn as reference, the gas metallicity for this DLA **turns out to be** $[\text{Zn}/\text{H}] = -1.10 \pm 0.05$ (or $Z_{\text{DLA}} = 1/12 Z_{\odot}$). **A slightly lower metallicity is obtained if Fe is used**, $[\text{Fe}/\text{H}] = -1.26 \pm 0.02$. For $z = 2$, this Fe abundance is quite at the upper end of current samples of DLA systems (Prochaska & Wolfe 2000), while the Zn value is much more representative of all measurements at $z \sim 2 - 2.5$ (Pettini et al. 1997; Vladilo et al. 2001). This is because $[\text{Zn}/\text{Fe}] > 0$ for the majority of the DLAs.

6.3. Dust content

The key property of the present DLA system is its apparent lack of dust. **We measure** $[\text{Zn}/\text{Cr}] = -0.01 \pm 0.05$, a value which is consistent with no dust-depletion, since Cr, unlike Zn, is depleted in the local ISM. Another check for the presence of dust is provided by the refractory elements Fe and Ni. The Zn/Fe and Zn/Ni ratios are expected to be supersolar if dust is present, because Fe and Ni are two of the most heavily depleted elements in the ISM. In addition, $[\text{Zn}/\text{Fe}] \approx 0$ for metal-poor stars of a wide range of metallicities (Gratton & Sneden 1991; Sneden, Gratton & Crocker 1991; but see the discussion in Prochaska et al. 2000), so any departure from this value could be attributed to dust depletion. **We observe** $[\text{Zn}/\text{Fe}] = +0.16 \pm 0.03$ and $[\text{Zn}/\text{Ni}] = -0.18 \pm 0.06$. **While the Zn/Fe ratio implies a certain degree of dust depletion, the Zn/Ni abundance gives further evidence in support of dust-free gas.** Altogether these 3 ratios indicate that the fraction of atoms that are missing from the gas phase is insignificant.

Nevertheless, these inferences all rely on the goodness of our zinc abundance, **which was not determined by profile fitting of the velocity components. An independent argument against significant dust depletion comes from the ratio** $[\text{S}/\text{Si}] = -0.06 \pm 0.03$. Since (a) these two elements have a common nucleosynthetic origin, and (b) silicon is normally depleted in the ISM while sulfur is not (Savage & Sembach 1996), one expects this ratio to be supersolar if dust were present in this DLA, which is not observed.

In conclusion, it seems that we have found a new DLA lacking dust, the second such instance at high redshift. Other cases of DLAs with small dust content are reported in Molaro et al. (2000), in Pettini et al. (2000), and in Prochaska & Wolfe (1999). From the Pettini et al. compilation the DLA with lowest dust content has $[\text{Zn}/\text{Cr}] = -0.13 \pm 0.20$ at $z = 0.86$ toward Q0454+039, and from Prochaska & Wolfe, $[\text{Zn}/\text{Cr}] = -0.20 \pm 0.12$ in the $z = 1.920$ DLA toward Q2206-199. In both cases, there appears to be some degree of dust depletion, at least stronger than in the present DLA. A more similar case as ours was reported by Molaro et al. (2000) who measured $[\text{Zn}/\text{Cr}] = -0.06 \pm 0.08$ at $z = 3.39$

toward Q0000-2620. **This shows that the present system is uncommon among the few documented low-dust DLAs.**

6.4. α /Fe-peak ratios

A diagnostic tool to probe the evolutionary stage in DLAs is the abundance ratio of α to Fe-peak elements. Due to their different origins, α -capture elements being produced mainly in SNe Type II, and Fe-peak elements being delivered to the ISM by SNe Type Ia on a longer timescale, the α to Fe-peak ratio is expected to rapidly attain supersolar values in a chemically less mature system. Moreover, this ratio should decrease as cosmic time proceeds, unless possible environmental factors might influence it (Ellison & Lopez 2001). In our Galaxy the values range from $\langle [\alpha/\text{Fe}] \rangle \approx +0.5$ in metal-poor stars down to ≈ 0 , as metallicity increases.

All α elements we measure in the DLA toward HE 2243–6031 follow each other quite closely (with the exception of Ar; see below). **We obtain $[\text{Si}/\text{Zn}] = +0.24 \pm 0.05$, and $[\text{S}/\text{Zn}] = +0.18 \pm 0.04$** (recall that silicon is normally depleted in the local ISM; Savage & Sembach 1996). Even the α -element oxygen, despite the larger measurement errors, fits well into the trend **with $[\text{O}/\text{Zn}] = +0.29 \pm 0.22$. On average, we obtain for Si and S $\langle [\alpha/\text{Zn}] \rangle = +0.21 \pm 0.06$** (simple mean). This value is in good agreement with measurements of metal-poor halo stars (e.g., Ryan et al. 1996 and references therein) or the thick disk (Prochaska et al. 2000) at $[\text{Fe}/\text{H}] = -1.2$, but is high when compared with the current sample of DLAs. The conclusion is: like in Galactic metal-poor stars, these ratios probably reflect the temporal delay between SNe of Type I and II. They show that, despite its high metallicity, this DLA gas has not undergone significant metal pollution from SN Type I yields. We re-emphasize that these ratios are **likely** unbiased from dust-depletion effects. Centurion et al. (2000) have used the $[\text{S}/\text{Zn}]$ ratio to investigate a possible evolution of the α /Fe-peak abundance ratio that is unbiased from dust effects. Although their sample is small (6 measurements) those authors do find a decrease in that ratio with increasing metallicity, which is what one would expect if metallicity keeps track of chemical evolution in DLAs and if the objects conform a chemically homogeneous sample. Our measure of $[\text{S}/\text{Zn}]$ does not fit in that trend, being too high for $[\text{Zn}/\text{H}] = -1.1$, but it much better conforms to the enhancement observed in metal-poor stars.

6.5. The odd-even effect

The odd-even effect, that is, the underabundance of odd- Z elements relative to even- Z elements of the same nucleosynthetic origin, is another known property of Halo stars. Since Fe is more prone to dust depletion than Mn in a variety of ISM environments, this ratio can be used as a discriminant between dust depletion and pure SN Type II

enrichment. In fact, $[\text{Mn}/\text{Fe}]$ averages ≈ -0.3 in Galactic Halo stars at $[\text{Fe}/\text{H}] = -1$ (Ryan et al. 1996), whilst $[\text{Mn}/\text{Fe}] \approx +0.3$ in the local ISM (Savage & Sembach 1996).

The Fe II-corrected value of our 3σ upper limit for the non-detection of Mn II yields $[\text{Mn}/\text{Fe}] < -0.51$, which confirms the odd-even effect, is in accordance with the sample of Halo metal-poor stars in Ryan et al. (1996), but is quite low for that of thick disk stars in Prochaska et al. (2000). The low value also conforms with previous DLA measurements (Lu et al. 1996).

We do not observe the same effect for P, the other odd-element observed in this DLA. **We obtain $[\text{P}/\text{Si}] = +0.10 \pm 0.09$ at $[\text{P}/\text{H}] = -0.8$. This value is high if compared with $[\text{P}/\text{Si}] = -0.40$ at $[\text{P}/\text{H}] = -2.3$ (Molaro et al. 2001) and $[\text{P}/\text{Si}] = -0.30 \pm 0.09$ at $[\text{P}/\text{H}] = -1.2$ (Outram et al. 1999).**

6.6. Underabundant Ar I

Our column density estimate for Ar I implies a significant underabundance of Ar with respect to other α -chain elements. This corresponds to ~ -0.5 dex of what is expected if argon is **overabundant by +0.2 dex** (assuming argon tracks α elements [Timmes, Woosley & Weaver 1995]). In the local ISM, Ar I is rarely found or is significantly below its cosmic abundance relative to H I (Sofia & Jenkins 1998; Jenkins et al. 2000). As suggested by Sofia & Jenkins in order to explain their finding of a low Ar I abundance in the local ISM, the underabundance can be explained if a significant part of the argon is ionized. In this DLA that fraction is $\sim 60\%$. Moreover, since Ar I has a much larger ionization cross section than H I, our measurement can also be explained in terms of moderately ionized gas, which brings Ar I into Ar II in higher proportions than for the rest of the low-ions. The alternative explanation, a low Ar I abundance caused by dust depletion, is in our DLA ruled out given (1) the scarce propensity of Ar to dust-grain incorporation (Meyer et al. 1991; Sofia & Jenkins 1998) and (2) the negligible amount of dust (6.3). Thus, these conditions resemble very much those in the local ISM described by Sofia & Jenkins where argon is systematically found underabundant, and confirm their suggestion that ionization, and not dust, is the responsible agent.

6.7. Nitrogen

Chemical evolution models predict the production of nitrogen in the CNO cycle in stellar interiors to have two different origins. While primary N is produced in intermediate-mass stars ($3 - 8 M_{\odot}$) without dependence on the initial metal content, secondary nitrogen is also produced in stars of any mass but with an initial supply of heavy elements. The net result is that the N/O ratio should be independent of O/H for primary N while $\text{N/O} \propto \text{O/H}$ for secondary N. In addition, since intermediate-mass stars evolve on much

larger scales than the short-lived progenitors of SN Type II – responsible for the bulk of α -elements like O, Si, S, etc. –, there should be a delay of $\sim 5 \times 10^8$ yr between the release of primary N and that of O (Lu et al. 1998 and references therein).

We measure $[N/O] = -1.03$ at $[O/H] = -0.81$. However, despite the accurate N abundance we were able to obtain, our oxygen estimate is rather uncertain.³ Relying rather on the better estimates for Si and S, we find $[N/Si] = -0.98$ at $[Si/H] = -0.86$ (**and basically the same values are found if S is used**). Referring to Fig. 1 in Lu et al. (1998), this value is at the very low end of DLA measurements at this Si abundance; moreover, according to the fits to Galactic measurements, it is better explained as secondary nitrogen⁴. This is in agreement with the high α /Fe-peak ratios we observe because both effects can be explained by an early phase in this protogalaxy’s chemical evolution, observed at a time when the release of Fe-peak elements and primary nitrogen has not yet begun.

7. Summary of the conclusions

1. We have studied in detail a $z = 2.33$ DLA observed at high resolution toward the bright QSO HE 2243–6031. We have been able to detect and obtain reliable column densities for H I, N I, Si II, P II, S II, Ar I, Cr II, Fe II, Ni II, Zn II, and Al III; less accurate determinations for C II, Al II and O I; and to put upper limits on Mn II, S III, Fe III, P III, and N II. **The metallicity of this system is $[Zn/H] = -1.1$.**
2. By comparing column densities of single velocity components we have performed the first cloud-by-cloud analysis in a high- z DLA so far. We find a tight correlation of all low-ionization species with respect to Fe II extending over 2.5 orders of magnitude in $N(\text{Fe II})$. We interpret this trend as a lack of significant **changes in the** dust, ionization, and intrinsic chemical-enrichment effects. If Fe II tracks H I, such homogeneity differs from what is observed in the local ISM, meaning that our line of sight probably samples clouds located in one single environment.
3. We find a probable scenario for the occurrence of Al III is ionized shells surrounding neutral cores of Al II. Photoionization models show that the ratio of Al III to low ions can be modeled with a wider range of higher ionization parameters than the ratio

³ Fig. 9 shows C8 departures from the trend followed by the other 4 components. This might be due to an overestimate of C8 (which dominates the total column density). Excluding C8 and re-scaling, however, implies lowering the total column density by 0.7 dex. Although such value conforms better with the rest of the components, it translates into $[O/H] = -1.5$, so the underabundance of N over O would become only $[N/O] = -0.2$.

⁴ **But let us note that N II could contribute with ≈ 0.20 dex to the nitrogen abundance, thus bringing $[N/Si]$ more in line with the Lu et al. values.**

among low ions. Independently of this, the disparate line width differences between Al II and Al III also support the notion of separate Al II and Al III regions.

4. Using different abundance ratios between ISM refractory and non-refractory elements we have shown that the observations are compatible with negligible amounts of dust in this protogalaxy, **although the measured $[\text{Zn}/\text{Fe}] = +0.16 \pm 0.03$ may indicate a small degree of dust depletion.**
5. We observe – unbiased by dust depletion effects – an enhancement of the α/Fe -peak **ratios of +0.2 dex** for various elements, a marked odd-even effect in Mn, and a strong underabundance of N relative to Si and S, $[\text{N}/\text{Si,S}] = -1$ at $[\text{Si}/\text{H}] = -0.86$. All of these ratios support an environment that is in an early evolutionary stage, where the onset star formation has begun shortly before the DLA was observed. The absence of dust is in agreement with this notion, if there has not been time enough to form dust grains.
6. The observed underabundance of Ar I by 0.5 dex is easily explained by a significant fraction of argon residing in a higher ionization phase. This situation resembles the conditions in the local ISM. Our ionization simulations demonstrate, however, such an ionized phase does not contain a considerable part of the other elements, so our abundance measurements are not affected by undetected ionized atoms.

7.1. Final comment

The observed uniformity of metal abundances across the line of sight to HE 2243–6031 has important implications for current models of galaxy formation. As mentioned before, it suggests the individual components are embedded in the same environment, which, in addition, must have undergone significant mixing. If DLAs are formed from the accretion of protogalactic small clumps (e.g., Haehnelt et al. 1998) that have formed independently, then one expects each protogalaxy to contribute with gas of different dust and nucleosynthetic compositions. The homogeneity of metal abundances observed in this DLA is difficult to explain in this scenario, unless the mixing of metals has occurred in short enough timescales to counteract the enhancement of any original differences (e.g., through the metal release by SN Type I; see the discussion in Prochaska & Wolfe 2002). The chemically young gas we apparently observe might be a consequence of such a rapid process.

Although the statistical weight of our result on single-cloud abundances may not be sufficient to draw any general conclusions on the physical nature of DLAs, the observed uniformity in HE 2243–6031 seems to be a quite common property among DLAs (Prochaska et al. 2001).

On larger physical scales, also important for constraining the models is to investigate abundance variations among systems. There are few known ‘DLA groups’ along single lines of sight where the redshift separation is small enough to support a physical connection between the DLAs, but big enough to characterize the systems as separate entities (i.e., a few 1000 km s⁻¹; Lopez et al. 2001; Ellison & Lopez 2001). In the only such groups so far investigated at high resolution, Ellison & Lopez (2001) find very similar relative abundances among the DLA members, despite their different metallicities. While it is not clear whether such DLA groups later merge, environment may be an effective catalyzer of metal enrichment in DLAs at early evolutionary stages.

Acknowledgements. We warmly thank Sara Ellison for her valuable comments on an earlier version of the paper; Ulysses Sofia for an informative discussion; Piero Madau and Francesco Haardt for having made available an updated version of their spectrum to us; Scott Burles for having taken the B&C spectrum of HE 2243–6031, and G. Vladilo, the referee, for a careful reading of the manuscript. JXP was supported by NASA through a Hubble Fellowship grant HF-01142.01-A awarded by STScI, and SL acknowledges financial support by FONDECYT grant N°3000 001 and by the Deutsche Zentralstelle für Arbeitsvermittlung.

References

- Bergeson S. D. & Lawler J. E. 1993a, ApJ 408, 382
 Bergeson S. D. & Lawler J. E. 1993b, ApJ 414, L137
 Boissé P., Le Brun, V. Bergeron, J., & Deharveng, J.-M., 1998, A&A 333, 841
 Cardelli, J. A. & Savage, B. D., 1995, ApJ 452, 275
 Centurion, M. Bonifacio, P., Molaro, P., & Vladilo, G., 2000, ApJ 536, 540
 Ellison, S. L. & Lopez, S., 2001, A&A submitted.
 Fedchak, J. A., Wiese, L. M., & Lawler, J. E., 2000, ApJ 538, 773
 Ferland, G. J. 1993, University of Kentucky, Physics Department Internal Report
 Fontana, A. & Ballester, P., 1995 The Messenger 80, 37
 Giallongo, E., Cristiani, S., D’Odorico, S., Fontana, A., & Savaglio, S. 1996, ApJ 466, 46
 Gratton, R. G., Sneden, C., 1991 A&A 241, 501
 Ge, J., Bechtold, J., & Kulkarni, V. P., 2001, ApJ 547, L1
 Haardt, F., & Madau, P. 1996, Apj 461, 20
 Haehnelt, M. G., Steinmetz, M. & Rauch, M. 1998, ApJ 495, 647
 Howk, J. C. & Sembach, K. R., 1999, ApJ 523, L141
 Howk, J. C., Sembach, K. R., Roth, K. C. & Kruk, J. W. 2000, ApJ 544, 867
 Jenkins, E. B., Oegerle, W. R., Gry, C., Vallerga, J., Sembach, K. R., Shelton, R. L., Ferlet, R., Vidal-Madjar, A., York, D. G., Linsky, J. L., Roth, K. C., Dupree, A. K., & Edelstein, J., 2000, ApJ 538, L81
 Levshakov, S. A., Kegel, W. H., & Agafonova, I. I., 2001 A&A, 373, 836
 Lopez, S., Maza, J., Masegosa, J., & Marquez, I., A&A 366, 387
 Lopez S., Reimers D., Rauch M., Sargent W. L. W. & Smette A., 1999, ApJ 513, 598

- Lu, L., Sargent, W. L. W., Barlow, T. A., Churchill, C. W., Vogt, S., 1996, *ApJS* 107, 475
- Lu, L., Sargent, W. L. W., & Barlow, T. A., 1998, *AJ* 115, 55
- Morton, D. C., 1991, *ApJS* 77, 119
- Morton, D. C., 1991, *ApJS* 77, 119
- McWilliam, A., 1997 *ARA&A* 35, 503
- Molaro, P., Levshakov, S. A., D’Odorico, S., Bonifacio, P., & Centurion, M., 2001, *ApJ* 549, 90
- Molaro, P., Bonifacio, P., Centurion, M., D’Odorico, S., Vladilo, G., Santin, P., & Di Marcantonio, P., 2000, *ApJ* 541, 54
- Outram, P. J., Chaffee, F. H., & Carswell, R. F., 1999, *MNRAS* 310, 289
- Pettini, M., Smith, L. K., King, D. L., & Hunstead, R. W., 1997, *ApJ* 486, 665
- Pettini, M., Ellison, S. L., Steidel, C. C., & Bowen, D. V., 1999, *ApJ* 510, 576
- Pettini, M., Ellison, S. L., Steidel, C. C., Shapley, A. E., & Bowen, D. V., 2000, *ApJ* 532, 65
- Press, W. H., Flannery, B. P., Teukolsky, S. A., & Vetterling, W. T. 1986, *Numerical Recipes*, Cambridge University Press.
- Prochaska, J. X. & Wolfe, A. M., 1996, *ApJ* 470, 403
- Prochaska, J. X. & Wolfe, A. M., 1999, *ApJS* 121, 369
- Prochaska, J. X. & Wolfe, A. M., 1997, *ApJ* 474, 140
- Prochaska, J. X. & Wolfe, A. M., 2000, *ApJ* 533, L5
- Prochaska, J. X., Naumov, S. O., Carney, B. W., McWilliam, A., & Wolfe, A. M., 2000, *AJ* 120, 2513
- Prochaska, J. X., Wolfe, A. M., Tytler, D., Burles, S., Cooke, J., Gawiser, E., Kirkman, D., O’Meara, J. M., & Storrie-Lombardi, L., 2001, *ApJS* 137, 21
- Prochaska, J. X., & Wolfe, A. M., 2002, *ApJ* in press.
- Reimers, D., & Wisotzki, L., 1997, *The Messenger* 88, 14
- Ryan, S. G., Norris, J. E., & Beers, T. C., 1996, *ApJ* 471, 254
- Savage, B. D. & Sembach, K. R., 1991, *ApJ* 379, 245
- Savage, B. D. & Sembach, K. R. 1996, *ARA&A* 34, 279
- Schechtman, R. M., Povolny, H. S., & Curtis, L. J. 1998, *ApJ* 504, 921
- Sofia, U. J. & Jenkins, E. B. 1998, *ApJ* 499, 951
- Snedden, C. Gratton, R. G., & Crocker, D. A. 1991, *A&A* 246, 354
- Spitzer, L. & Fitzpatrick, E. L., 1995, *ApJ* 455, 196
- Storrie-Lombardi, L. J., & Wolfe, A. M., 2000, *ApJ* 543, 552
- Timmes, F. X., Woosley, S. E., & Weaver, T. A., 1995, *ApJS* 98, 617
- Tytler, D., & Fan, X.-M. 1992, *ApJS* 79, 1
- Verner, D. A., Barthel, P. D. & Tytler, D., 1994, *A&AS* 108, 287
- Vidal-Madjar, A., Kunth, D., Lecavelier des Etangs, A., Lequeux, J., André, M., BenJaffel, L., Ferlet, R., Hébrard, G., Howk, J. C., Kruk, J. W., Lemoine, M., Moos, H. W., Roth, K. C., Sonneborn, G., & York, D. G., 2000, *ApJ* 538, L77
- Viegas, S. M., 1995 *MNRAS*, 276, 268
- Vladilo, G., 1998 *ApJ* 493, 583
- Vladilo, G., Centurión, M., Bonifacio, P., & Howk, J. C., 2001, *ApJ* 557, 1007

Vladilo, G., Bonifacio, P., Centurión, M., & Molaro, P., 2000, ApJ 543, 24

Wakker, B. P., & Mathis, J. S., 2000, ApJ 544, L107

Welty, D. E., Hobbs, L. M., Lauroesch, J. T., Morton, D. C., Spitzer, L., & York, D. G., 1999, ApJ 124,465

Welty, D. E., Frisch, P. C., Sonneborn, G., & York, D. G., 1999, ApJ 512,636

Wolfe, A. M., 1993, Ann. NY Acad. Sci. 668, 281

Wolff, B., Koester, D., & Lallement, R. 1999, A&A 346, 969